Advances in Computational Design, *Vol. 5, No. 1 (2020) 35-54*
DOI: https://doi.org/10.12989/acd.2020.5.1.035

Relationships for prediction of backstay effect in tall buildings with core-wall system

Mahdi Karimi[1a], Ali Kheyroddin*[1] and Hashem Shariatmadar[2b]

[1]*Department of Civil Engineering, Semnan University, Semnan, Iran*
[2]*Department of Civil Engineering, Ferdowsi University of Mashhad, Mashhad, Iran*

(Received February 10, 2019, Revised July 12, 2019, Accepted September 28, 2019)

Abstract. One of the prevailing structural systems in high-rise buildings is the core-wall system. On the other hand, the existence of one or more underground stories causes the perimeter below-grade walls with the diaphragm of grade level to constitute of a very stiff box. In this case or a similar situation, during the lateral response of a tall building, underground perimeter walls and diaphragms that provide an increased lateral resistance relative to the core wall may introduce a prying action in the core that is called backstay effect. In this case, a rather great force is generated at the diaphragm of the grade-level, acting in a reverse direction to the lateral force on the core-wall system, and thus typically causes a reverse internal shear. In this research, in addition to review of the results of the preceding studies, an improved relationship is proposed for prediction of backstay force. The new proposed relationship takes into account the effect of foundation flexibility and is presented in a non-dimensional form. Furthermore, a specific range of the backstay force to lateral load ratio has been determined. And finally, it is shown that although all suggested formulas are valid in the elastic domain, yet with some changes in the initial considerations, they can be applied to some certain non-linear problems as well.

Keywords: backstay effect; core-wall; concrete box; stiffness ratio; shear deformation; foundation flexibility

1. Introduction and goal

High-rise buildings are being deployed around the world more and more often nowadays. The growth in construction of modern tall buildings, however, which began in the 1880s, has been largely for commercial and residential purposes (Smith and Coull 1991). In this situation, an economic, optimum, and proper plan for designing the structural system of such a building is one of the most important factors that a good design must contain. Within the existing structural resisting systems, shear walls are widely used for both tall buildings and low-rise buildings. They are important structural members used in the lateral resisting system. There are two major types of cores: concrete core and steel framed cores. Reinforced concrete cores are a more standard option

*Corresponding author, Professor, E-mail: kheyroddin@semnan.ac.ir
[a] Ph.D. Student, E-mail: Mkarimi@semnan.ac.ir
[b] Associate Professor, E-mail: Shariatmadar@um.ac.ir

http://www.techno-press.org/?journal=acd&subpage=7 ISSN: 2383-8477 (Print), 2466-0523 (Online)

for tall buildings in general, as seen from the history, concrete structure is dominant in the market because they provide more stiffness than steel cores, and it is relatively cheaper to use a concrete core in certain countries such as China (Fu 2018). Another reason that makes the core-wall system the best choice is the straightforward accommodation to architectural plan due to fitting to stairs box and elevators and usually being located somewhere around the center of the plan. On the other hand, another important aspect of structural design of tall buildings is the below-grade problems. Once a high-rise building is considered to be designed, number of building basements is usually dictated by architectural issues and the question of "what aspects of structural design must be considered?" is less considered. This consists of foundation type, soil conditions, soil structure interaction (SSI), system overturning, and a less attended subject named "Backstay Effects" and so forth. Existence of basements also leads to increasing of structural fixation. In this regard, the entering depth of structure to the ground sometimes is referred to as "Embedment Length".

Many factors may influence the demand shear or moment of a core-wall component. For example the effect of near-fault and far-fault ground motion on shear, moment and energy demand of core-walls has been investigated by Beiraghi *et al*. (2016) and Beiraghi (2018a, b, c). Earthquake effects on the core-wall system combined with other systems, also have been investigated by Beiraghi and Siahpolo (2016) and Beiraghi (2017, 2018d). The effect of the placement and the various configurations of shear walls in slender tall buildings were investigated by Farghaly (2016). According to the outcomes of his research, when the shear walls are not in the entire building height, the results show high values of stresses at the ends of the shear walls. A good discussion on the merits of the core-wall system and important issues about the modeling techniques of tall buildings has been performed by Fu (2018, 2015). This research, however, is concerned about the influence of backstay effects that can considerably change the shear and moment of a core-wall. Generally, this phenomenon is most noticeable in buildings that a portion of lateral system is disrupted and does not continue to top of the building. Hence, existence of any setback at the height of a building can generate this effect. However, the present paper focuses on a high-rise building with a core-wall system and containing subterranean levels, where backstay effect is occurred due to restraint at the grade level (Fig. 1).

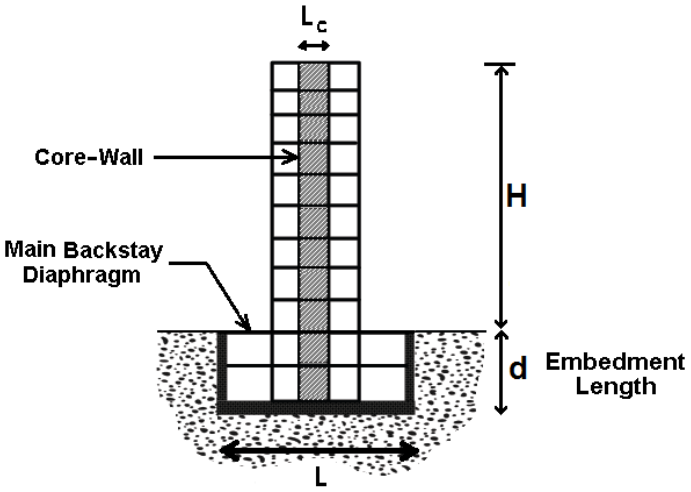

Fig. 1 A tall building with effective components in backstay phenomenon (Karimi and Kheyroddin 2016)

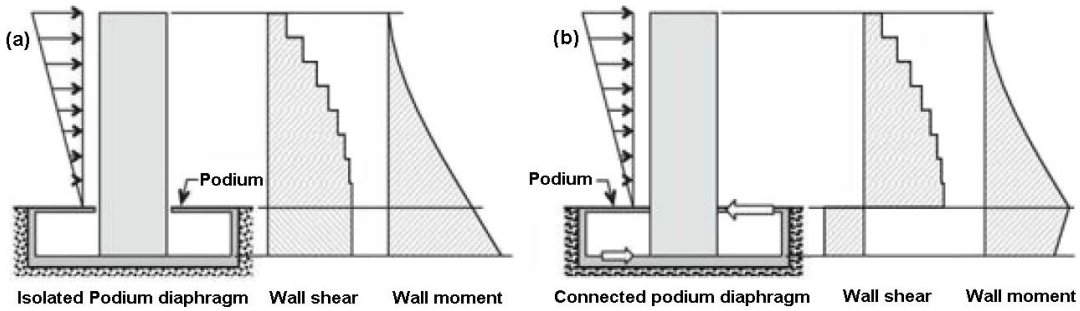

Fig. 2 Backstay effect: (a) wall and podium diaphragm not connected; (b) wall and podium diaphragm connected (Moehle 2015)

According to the definition presented in TBI/PEER (2017) and LATBSDC (2017) the backstay effect is the set of lateral forces developing within a podium structure to equilibrate the lateral forces and moment of a tower extending above the podium structure. This condition is common to tall core-wall buildings in which the core extends into a stiff basement structure braced by stiff basement walls around the perimeter (TBI/PEER 2017, LATBSDC 2017).

In brief, a conceptual description of backstay effects can be explained so: for a typical building with one or more below-grade levels, the perimeter basement walls create a very large and laterally stiff box. The ground floor diaphragm engages this box and integrates it into the lateral system. This results in shedding of lateral load from the main lateral force resisting system (in this research shear wall or core-wall system) to the basement walls (Tocci and Levi 2012). Due to large magnitude of the created force, the generated reaction force may reverse the shear internal force of a core-wall. This action sometimes is referred to as the backstay effect. The term "flagpole effect" sometimes is used as well (Moehle 2015). Fig. 2 illustrates the preceding description of backstay effect in a pictorial presentation. This figure illustrates the backstay effect on the wall shears and moments. In Fig. 2a, the wall is isolated from the podium slab by a movement joint. Thus, wall shear is constant (ignoring additional inertial force in subterranean levels) and wall moment increases linearly to the foundation mat, where the mat is required to resist the entire wall shear and moment. In Fig. 2b, the wall and podium slab are connected, developing a backstay force that may result in wall shear reversal with corresponding reduced wall moments.

Fig. 2a also can be imagined as a limit state, where the lateral stiffness of the mentioned concrete box is close to zero. Investigation of variety of limit states (conditions that the stiffness of concrete box or foundation approaches to zero or infinity) was performed by Karimi and Kheyroddin (2016) by assumption of various boundary conditions. In this aforesaid study, shear and moment diagrams were dimensionless and normalized to its corresponding quantity at the base of structure.

Due to the complexity of capturing backstay effects in the analysis, it may be desired to eliminate the phenomenon in the actual buildings. This can be accomplished by isolating the lateral force resisting system from the foundation elements by providing lateral movement joint at the backstay diaphragms. Typically, this is done by providing a corbel or a similar detail at the diaphragm to shear wall interface (Tocci and Levi 2012). Although this idea may lighten the designer of structural system from many of challenges and complexities but is not considered as the best way compared to connecting diaphragm to shear wall or core-wall system. The latter (connected condition) is generally preferred since it (Fig. 2b) provides a redundant force path

(backstay force plus shear and moment at foundation mat) and also, because the lateral displacements of the wall and podium diaphragm are compatible (Moehle 2015).

However, the first solution has been utilized in designing of some actual buildings in some instances. As an egregious example for application of this method is in the Central Plaza Hong Kong high-rise building (Taranath 2010, Kowalczyk and *et al. 1995*). This building has 78 stories and a triangular plan. The lateral system for the tower consists of core shear wall with external façade frames acting as a tube. In order to reduce large shear reversals in the core-walls, the floor slabs and beams are separated horizontally from the core-walls at certain levels (Taranath 2010).

Following the preceding discussions and since the isolating method is not preferred for resolving the complexity of backstay effects, this research tends to provide relationships for predicting the backstay effects based on relative stiffness of structural elements comprising basement, core-wall, and foundation. In the subsequent sections, after reviewing the suggested recommendations of some reports and also the results from the previous researches, the latest proposed formulation for prediction of backstay effect (backstay force) including the foundation flexibility is presented.

2. Review of literatures

According to the result of one previously performed investigation, the reverse shear force below the flexural plastic hinge (the hinge at the location above the podium level) may be much larger than the base shear above the flexural hinge, depending on the stiffness of floor diaphragms and on the shear rigidity and flexural rigidity of the high-rise concrete walls (Adebar 2008). Another study indicates that increasing the quantity of horizontal reinforcement in the wall to above a certain limit may not prevent a shear failure, and thus a different design solution is to be found. Moreover, an upper-bound estimate of floor diaphragm stiffness should be used in order to not underestimate the shear strain demand on high-rise walls (Rad and Adebar 2009). Attention to capturing of backstay effects also has been considered by some reports and guidelines. The common approach for accounting for this phenomenon is playing with the stiffness of comprising components of below-grade structure by changing the effective stiffness via designated of recommended reduction factors. Those considered guidelines such as PEER/ATC-72-1 (2010) and LATBSDC (2017) recommend some values for upper and lower bounds for the stiffness of components influencing the backstay effects. This approach is typically referred to as bracketing. Elements contributing to backstay effects must be designed for critical conditions that are created by changing the recommended stiffness of those mentioned components.

Utilization of bracketing approach originates from the uncertainty and changing the mechanical behavior of structural components at earthquake time. For the case of reinforced concrete components, a number of variables can affect concrete stiffness properties, including: cracking, strain penetration, bond slip, panel zone deformation, and tension shift associated with shear cracking (PEER/ATC-72-1 2010). Although employing the recommended method in the aforementioned reports, may be a sufficiently confident way for accounting for the backstay effect, there is no factor responsible for the phenomenon can be assessed or estimated before modeling and analyzing the computational model of the structure. Due to this reason, some researches were conducted by the authors of the current article in a gradual procedure. In this procedural investigation, parameters affecting the backstay effects have been considered. Obtained results may help structural designer to increase his insight and engineering judgments, leading to a better decision for below-grade aspect ratio of the structure.

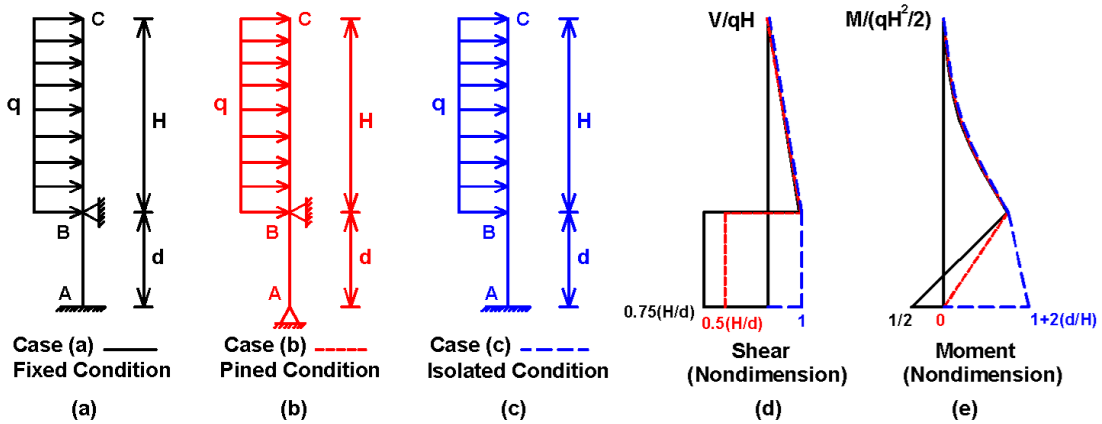

Fig. 3 Normalized diagram of shear and moment in considered of limit states (Karimi and Kheyroddin 2016)

2.1 Inspection of limit states

Limit States may be imagined as an extremely upper and lower bound that the stiffness of concrete box and other boundary conditions of the core-wall can be involved. Considering these limit states can improve the vision of the structural engineer. Fig. 3 shows three limit state of conditions under a uniformly distributed lateral load that is often used to simulate wind loading (Smith and Coull 1991). The first case (Fig. 3a) is related to a very stiff diaphragm and surrounding walls, comprising a fully stiff box and also a fully stiff foundation. This case has been simulated by a rigid support at grade level and a fixed support at base that prevents the rotation of core-wall end. The second (Fig. 3b) shows a similar case to the first one except for replacing the fixed support by a pined one. Latter is equivalent to a fully stiff box but a very flexible foundation. Finally, the third case (Fig. 3c) can be equivalent to the elimination of backstay effect by isolating the core-wall (refer to Fig. 2a) from lateral movement of diaphragm.

The shear and moment diagram of structure have been calculated and normalized to base shear and moment (shear and moment exactly above of grade level) of structure and has been represented in Fig. 3d and 3e respectively. These results have been obtained by the assumption that the core section property in the below-grade level is not varied over the height. Furthermore, in this calculation the shear deformation of below-grade portion of structure has been neglected. Consideration of shear deformation can lead to decreasing of below-grade shear and a more uniformly distribution of below-grade moment. This can be indicated by a comprehensive relationship that will be presented in the subsequence sections. It is noteworthy that the top portion of structure is in isostatic condition, and the section properties of this portion do not have any role in the obtained results from this study. It definitely is obvious that the distribution of lateral loads must be considered in this concern.

2.2 Simple model for assessment of backstay effects

After attaining the limit states aspects of the various conditions of backstay effect, replacing the support located at-grade level by a spring can represent a better vision of the backstay effect

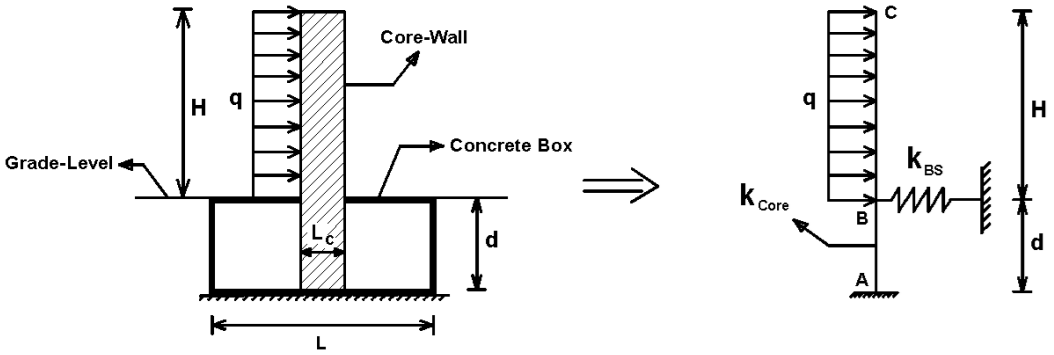

Fig. 4 Simple Model for Assessment of Backstay Effects (Karimi and Kheyroddin 2016)

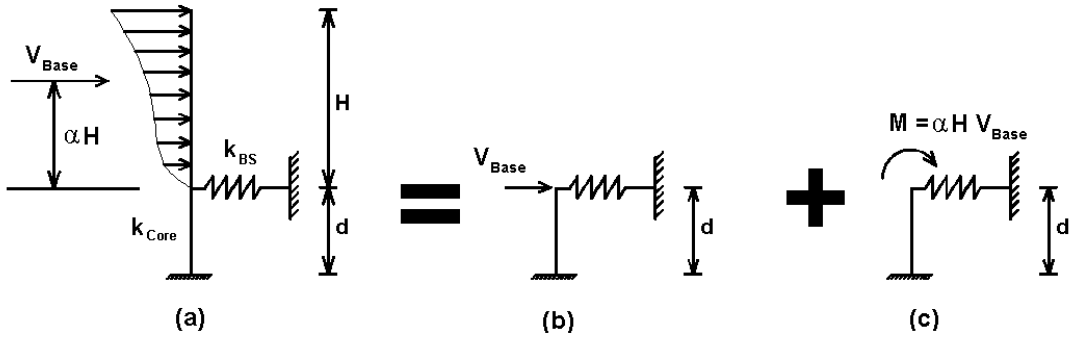

Fig. 5 Simple model for backstay formulation with the superposition law: (a) Model with the effect of load distribution; (b) Effect of load measure; (c) Effect of load distribution (Karimi and Kheyroddin 2016)

phenomenon now. The swapped spring will have the role of the concrete box. This simplified equivalent system has been illustrated at Fig. 4.

As shown in this figure, the entire lateral load has been supposed to be applied directly to the core-wall. This is true (not exact) when overhanging beams are pinned connections at its ends. Furthermore, it must be quoted that the existence of lateral load just above the grade level can be real only for wind kind of loading; therefore, in the case of seismic load it is merely correct for the case when the inertia force in subterranean level is ignored. This assumption has been made in the formula development process in this section and in all other subsequent progresses. Since the top portion of structure is in isostatic condition, the lateral load distribution can be substituted with an equivalent load system of a single force and moment. This can help generalize the subsequent obtained relationships. Fig. 5 shows the new equivalent model and also the usage of superposition law. In this figure, V_{Base} represents the total lateral load and α represents the effect of load distribution. Moreover, the generated force in the spring (F_{BS}) will denote the backstay force generated at the main backstay diaphragm. It should be noted that in general, the main backstay diaphragm located at the top of the podium perimeter walls will transfer more force than any other diaphragm PEER/ATC-72-1 (2010); therefore, for the formulation of backstay effect in this present research, effect of other diaphragms has been ignored.

Solving the one redundant degree system presented in Fig. 5a, and then normalizing it to the base shear gives the following relationship (Karimi and Kheyroddin 2016):

$$\frac{F_{BS}}{V_{Base}} = \frac{1 + 1.5\alpha\left(\frac{H}{d}\right)}{\frac{K_{Core}}{K_{BS}} + 1} \tag{1}$$

Where α is the relative distance of the center of lateral load to the grade level ($0 \leq \alpha \leq 1$), H is the height of the superstructure, d is the embedment length of structure in the ground, K_{Core} is the stiffness of core-wall, and K_{BS} is the stiffness of the concrete box (the box comprised of diaphragm of grade level and surrounding walls). These parameters also are depicted in Fig. 5.

In this formulation, the shear deformation of the core-wall has been neglected and therefore K_{Core} is obtained from the following relationship:

$$K_{Core} = \frac{3EI}{d^3} \tag{2}$$

Where E and I are elasticity modulus of core material and cross section moment of inertia in the below-grade portion of the core, respectively.

Eq. (1) shows that once the stiffness of K_{BS} relative to K_{Core} is large, the backstay force F_{BS} is increased. By increasing K_{BS} to infinity, the Eq. (1) approaches to the limit state of Fig. 3 case (a).

The verification of Eq. (1) has been established by examination of a building containing 21 total stories (with a typical story height of 3.5 meters) and one basement story with surrounding walls (H/d=20), illustrated in Fig. 6. ETABS program was utilized for assessment of this verification. Since the shear deformation has been ignored in obtaining Eq. (1), the shear stiffness of core-wall should be infinite in the numerical simulation. This is accomplished by multiplying the shear stiffness components of shell elements by a very high value, which is possible by changing the stiffness modification factors of shell elements within the ETABS program. In addition, in order to impose the entire lateral loads to the core-wall, all the beams of superstructure and a few columns were released from moments at their ends. Total lateral load was 210 tons (with a uniform distribution) and the created reversal shear force of core at below-grade, obtained from numerical analysis was 61 tons. Therefore, the result of the numerical analysis will be:

$$\frac{F_{BS}}{V_{Base}} = \frac{210 + 61}{210} = 1.286 \tag{3}$$

In order to calculate the result using Eq. (1), the core and concrete box stiffness (K_{Core} and K_{BS}) were required. These stiffness values were calculated from distinct models, as shown in Fig. 7. This stiffness can be obtained by applying a lateral uniform load to the edges of the core and concrete box interface separately and measuring the produced deformation at this location.

The result was:

$$\frac{K_{Core}}{K_{BS}} = 11.4 \tag{4}$$

Now with substituting specified values into Eq. (1), the result of the analytical relationship is given as:

$$\frac{F_{BS}}{V_{Base}} = \frac{1 + 1.5\alpha\left(\frac{H}{d}\right)}{\frac{K_{Core}}{K_{BS}} + 1} = \frac{1 + 1.5 \times 0.5 \times 20}{11.4 + 1} = 1.290 \tag{5}$$

Comparison of above value with the numerical result shows a good compatibility.

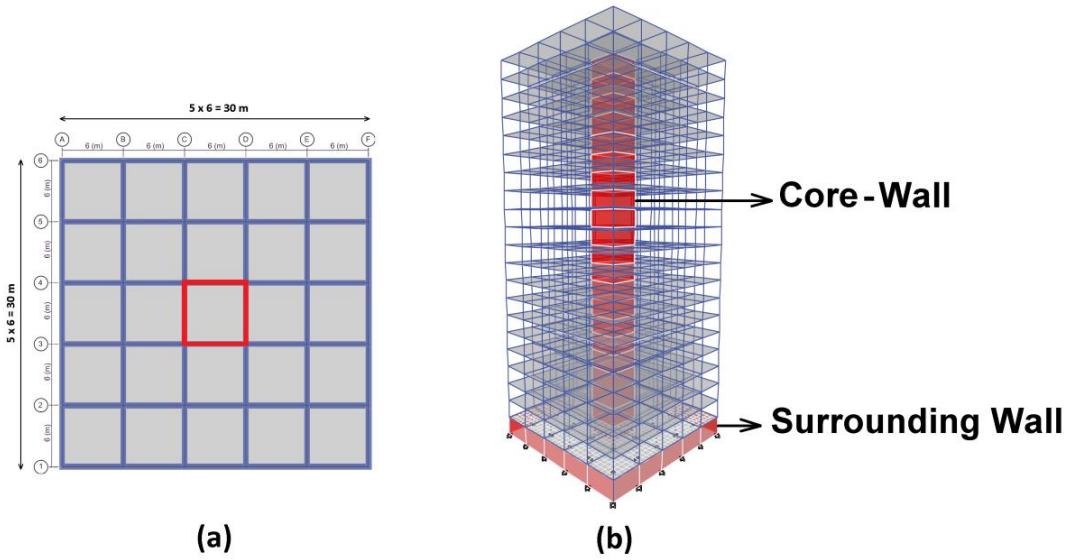

Fig. 6 Illustration of the model utilized for numerical verification by ETABS program with one story basement: (a) Plan of typical stories; (b) 3D view of model (Karimi and Kheyroddin 2016)

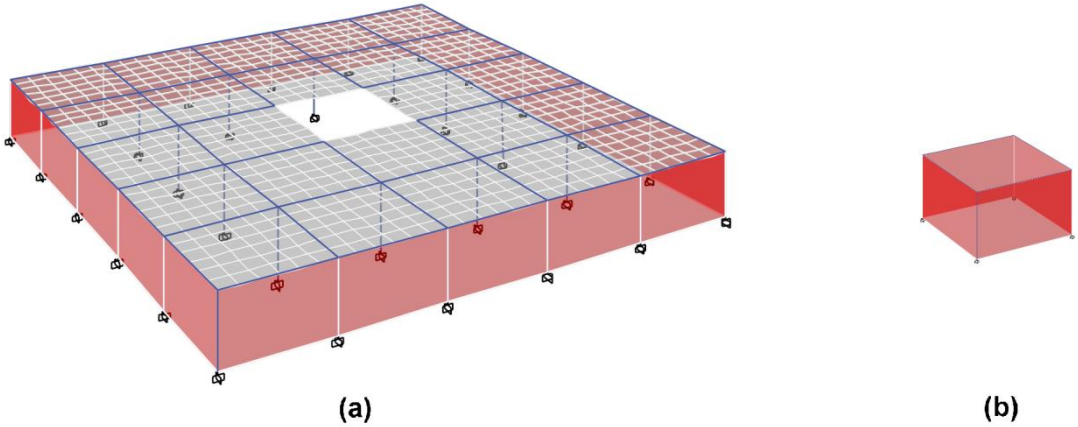

Fig. 7 Modeling of the bottom portion of the numerical model for the measuring of its stiffness; (a) Concrete box; (b) Core-wall (Karimi and Kheyroddin 2016)

2.3 *Improvement of presented formula by Including the Shear Deformation*

Although the presented relationship in the previous section has a good matching in the verification stage, it does not play a significant role in practical situations due to ignoring the shear deformation. This is caused by the large depth of the core section (L_C in Fig. 1) relative to the length of core element (embedment length or d in Fig. 1) in usual practical cases. Therefore, the result of another research (Karimi *et al*. 2018) considering the shear deformation is presented in this section.

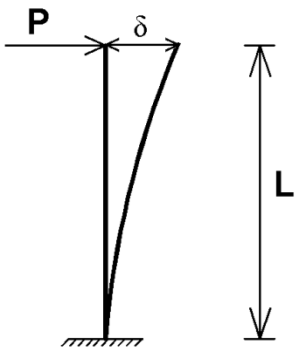

Fig. 8 Cantilever frame element under a concentrated force at the end

As can be seen in Fig. 8, total deformation of a cantilever column under a concentrated force P at its top can be written as:

$$\delta = \delta_b + \delta_s = \frac{PL^3}{3EI} + \frac{PL}{KAG} \tag{6}$$

Where, δ_b is bending deformation, δ_s is shear deformation, L is the length of column, A is the cross section area, I is the cross section moment of inertia, E and G are the young's modulus and shear modulus of material, and K is the shear area factor given by the following Equation (Gere and Timoshenko 1991):

$$K = \frac{I^2}{A\int_A \frac{Q^2}{t^2} dA} \tag{7}$$

in which t is the fiber length of the cross section at its location and Q is the first-order moment of area located above the considered fiber relative to the central area of the section. The value of K for a rectangular cross-section is 5/6.

Factorizing from bending stiffness term in Eq. (6) gives:

$$\delta = \delta_b + \delta_s = \frac{PL^3}{3EI} + \frac{PL}{KAG} = \frac{PL^3}{3EI}\left(1 + \frac{3}{K} \times \frac{E}{G} \times \frac{I}{AL^2}\right) \tag{8}$$

If the second term within the parentheses of Eq. (8) that reflects the shear deformation is considered as a new variable β,

$$\beta = \frac{3}{K} \times \frac{E}{G} \times \frac{I}{AL^2} \tag{9}$$

then Eq. (8) can be rewritten in a simpler form:

$$\delta = \delta_b + \delta_s = \frac{PL^3}{3EI} + \frac{PL}{KAG} = \frac{PL^3}{3EI}(1 + \beta) \tag{10}$$

In the β equation (Eq. (9)) K and I/A depend on cross section properties only, and E/G is dependent on the material type.

Now if for a particular section, β is designated, the total stiffness of a cantilevered frame element under a concentrated force can be specified as:

$$K_{CantileverT} = \frac{3EI}{L^3(1+\beta)} \tag{11}$$

Solving again the structural system of Fig. 5a and including the shear deformation, a more realistic of backstay effect can be represented. Solving the mentioned system leads to the following relationship:

$$\frac{F_{BS}}{V_{Base}} = \frac{1 + 1.5\frac{\alpha}{1+\beta}\left(\frac{H}{d}\right)}{\frac{K_{CoreT}}{K_{BS}} + 1} \tag{12}$$

Where, K_{CoreT} is the total stiffness of the core-wall by involving the shear deformation and can be obtained from Eq. (11) or via finite element analysis of the bottom portion of the core-wall.

Regarding Eq. (2) and Eq. (11), the following resulted relation may be noticeable:

$$K_{CoreT} = \frac{k_{Core}}{1+\beta} = \frac{3EI}{d^3(1+\beta)} \tag{13}$$

In order to determine the efficiency of β, if calculated for a simple section example of a thin walled square, it can represents the effect of core width (L_C at Fig. 1) to the depth of embedment length (d) aspect ratio. Therefore, supposing the Poisson's ratio of the reinforced concrete equal to 0.2, it will become:

$$\beta = 2.4\left(\frac{L_c}{d}\right)^2 \tag{14}$$

For a better illustration of d to L_C aspect ratio efficiency in the case of a thin walled square section, the ratio of F_{BS}/V_{Base} versus d/L_C has been presented in Fig. 9 for individual stiffness ratios of K_{BS}/K_{CoreT}. This figure is related to an H/d ratio of 20 and α=0.5, that had been used in numerical study of section 2-2.

As shown in Fig. 9, when d/L_C increases (shear deformation importance decreases) and with a simultaneous increase in K_{BS}/K_{CoreT}, F_{BS}/V_{Base} increases to the upper limit of the first case considered in section 2-1.

The same previous numerical study is applied for verification of Eq. (12) except for consideration of the shear deformation. In this case, since the shear deformation is taken into account, there was no need for multiplication of shear stiffness components of shell elements by any value.

With this new consideration, the result obtained from numerical analysis is as follows:

$$\frac{F_{BS}}{V_{Base}} = \frac{210+36}{210} = 1.171 \tag{15}$$

Where the value of 36 is the reversal shear force of core beneath the below-grade level.

Now and with the previous values from the case study using a particular value of β:

$$\beta = 2.4\left(\frac{L_c}{d}\right)^2 = 2.4\left(\frac{6}{3.5}\right)^2 = 7.05 \tag{16}$$

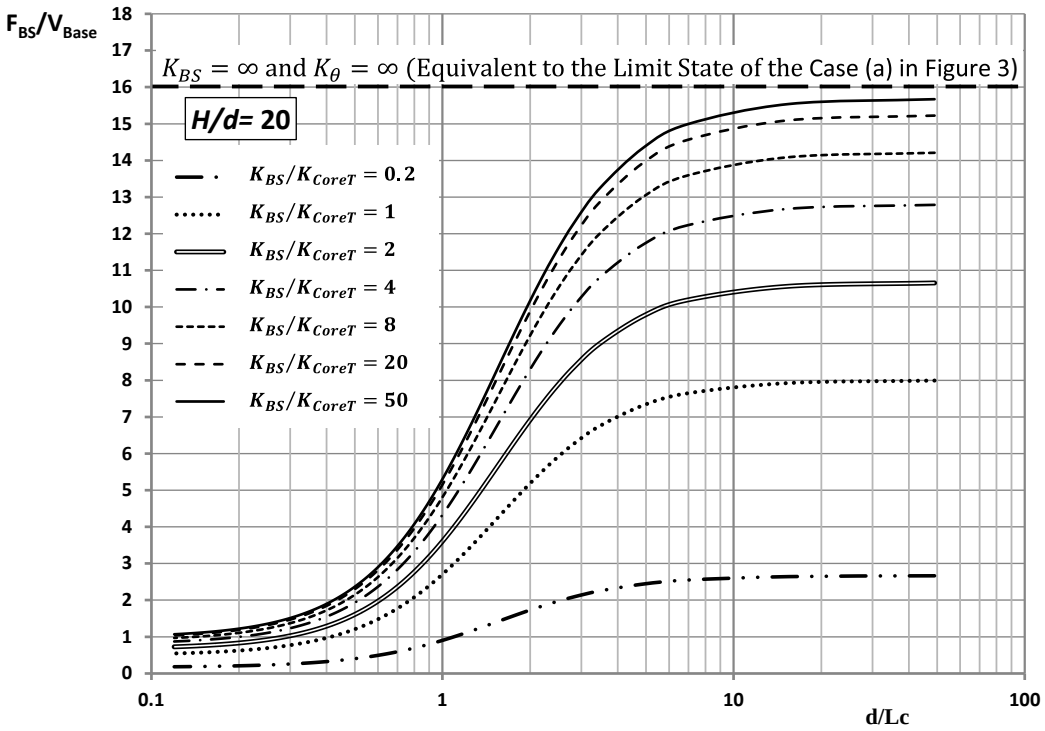

Fig. 9 Effect of shear deformation on backstay effect for a thin walled quadrilateral section with the length of L_C for the core-wall

the result obtained via the new relationship Eq. (12), can be written as:

$$\frac{F_{BS}}{V_{Base}} = \frac{1 + 1.5\frac{\alpha}{1+\beta}\left(\frac{H}{d}\right)}{\frac{K_{CoreT}}{K_{BS}} + 1} = \frac{1 + 1.5 \times \frac{0.5}{1+7.05} \times 20}{\frac{11.4}{(1+7.05)} + 1} = 1.185 \tag{17}$$

The comparison of the obtained results from the numerical analysis and the analytical relationship shows satisfactory close values.

3. Effect of foundation flexibility

In order to develop and further improve the last obtained relation (Eq. (12)), the foundation flexibility effect is considered. The foundation flexibility causes a partial rotation of core bottommost end and therefore, the assumption of non-fixed condition of core bottom end must be involved in this new consideration (the soil backfill behind the foundation perimeter wall may be considered by including the backfill soil stiffness via modifying K_{BS}). For reaching to the defined target, a rotational spring with stiffness of K_θ is inserted in the place of foundation and soil together as illustrated in Fig. 10. Solving this new structural system leads to achievement of a more general relationship for predicting the backstay effect.

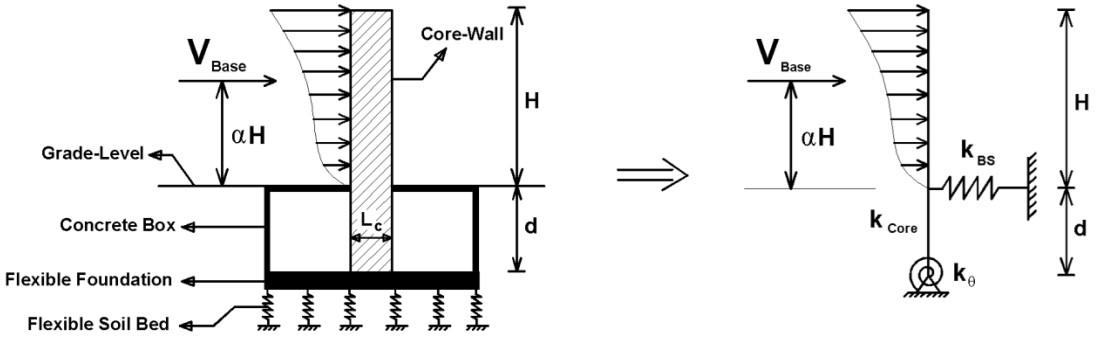

Fig. 10 New model for consideration of foundation flexibility in backstay effect

Formula obtained from solving the aforementioned system is given by:

$$\frac{F_{BS}}{V_{Base}} = \frac{1 + \frac{1.5+\gamma}{1+\beta+\gamma}\alpha\left(\frac{H}{d}\right)}{1 + \frac{K_{Core}}{K_{BS}(1+\beta+\gamma)}} \tag{18}$$

Eq. (18) can also be represented as a function of total stiffness of core-wall (K_{CoreT}) by substituting Eq. (13) into the latter equation:

$$\frac{F_{BS}}{V_{Base}} = \frac{1 + \frac{1.5+\gamma}{1+\beta+\gamma}\alpha\left(\frac{H}{d}\right)}{1 + \frac{K_{CoreT}}{K_{BS}} \times \frac{1+\beta}{1+\beta+\gamma}} \tag{19}$$

Where the new parameter of γ is the relative rotational stiffness of core-wall to its own foundation and can be obtained from the following equation:

$$\gamma = \frac{\frac{3EI}{d}}{K_\theta} \tag{20}$$

Where 3EI/d may be interpreted as rotational stiffness of a core-wall that means the required moment produced by p (M=Pd) for generation of one rad rotation of a cantilever element chord as illustrated in Fig. 11.

Other forms of Eq. (20) also can be rewritten as:

$$\gamma = \frac{\frac{3EI}{d}}{K_\theta} = \frac{\frac{3EI}{d^3}}{\frac{K_\theta}{d^2}} = \frac{K_{Core}}{\frac{K_\theta}{d^2}} \tag{21}$$

A first glance at the new relationship (Eq. (18) or Eq. (19)) together with Eq. (21) enlightens the fact that when K_θ approaches to infinity, γ approaches to zero and so the Eq. (18) or Eq. (19) are converted to the case of fixed support condition or the same as Eq. (12). For a better vision, the variation of F_{BS}/V_{Base} is shown in Fig. 12 for the constant values of H/d=20, β=7.05, and a uniformly distributed lateral load (α=0.5).

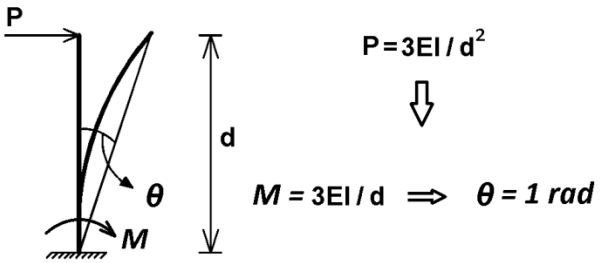

Fig. 11 Illustration for interpreting the rotational stiffness of a core-wall

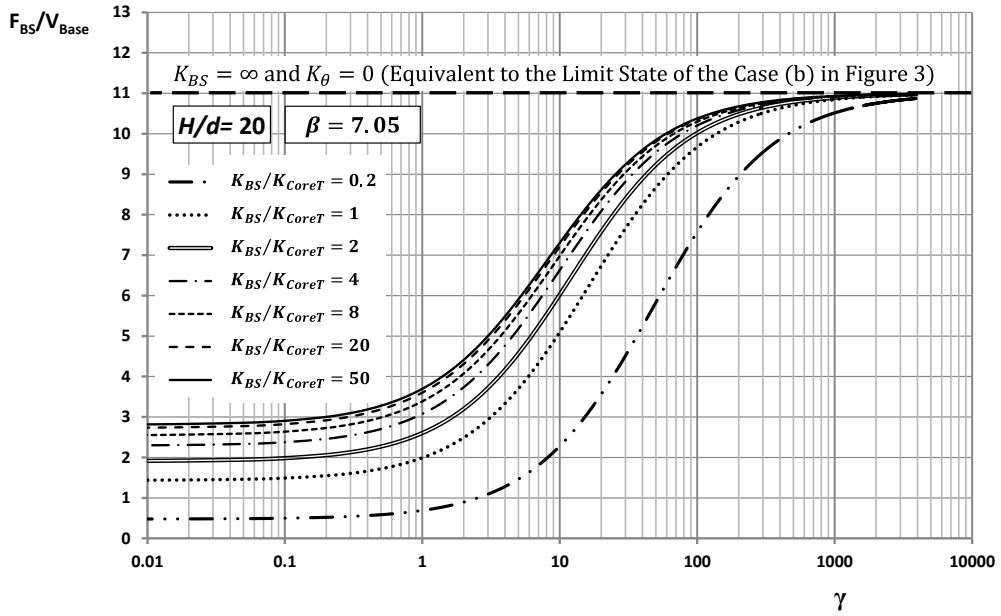

Fig. 12 Foundation flexibility effect on the backstay force ratio as an example case of specific values for other each parameter

3.1 Verification of the new obtained relationship

The same previous model with a difference in the embedment length of d=7m (two times of the typical story height) is considered for the sake of verification. This model is once tested with a rigid foundation (fixed conditions for the bottom end of the core and columns) and another time with a flexible foundation on a flexible soil bed, using the previous and the new relationship respectively. The height of flexible foundation is assumed to be equal to 1 meter, and the coefficient of soil subgrade reaction is supposed as 2 Kgf/cm^3. These assumptions provide a rather high flexibility condition; and thus a considerable difference may be expected from obtained results in comparison with the fixed condition. Analysis of the explained models showed a reverse shear of 240 ton and 699 ton for the cases of fixed condition and the flexible bed condition respectively. Therefore, the ratio of the generated backstay force to the total lateral load for the two mentioned cases can be written as:

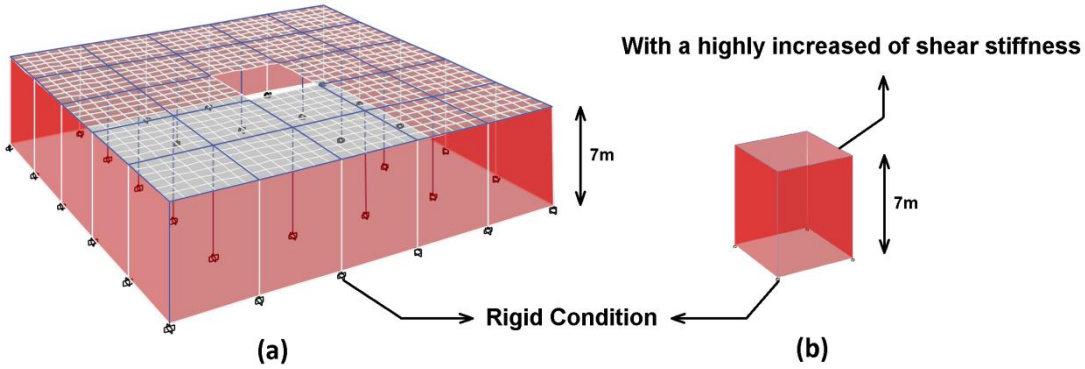

Fig. 13 Modeling of the bottom portion of the new numerical approach for measurement of its stiffness in the case of rigid base condition; (a) Concrete box; (b) Core-wall

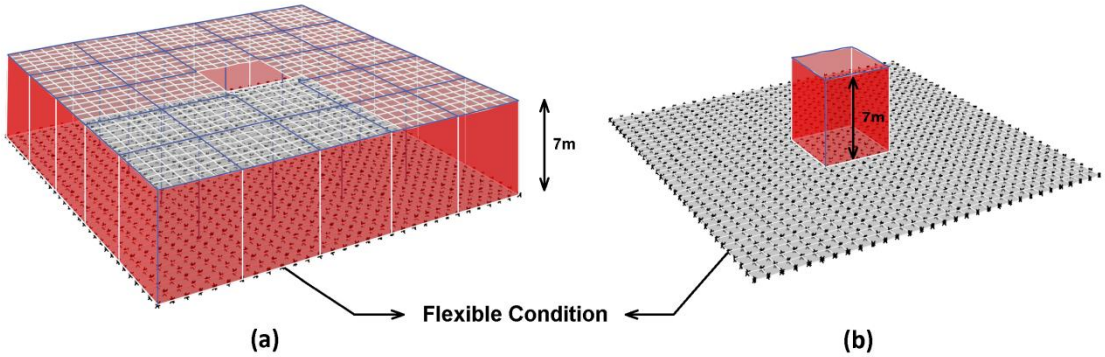

Fig. 14 Modeling of the bottom portion of the new numerical approach for measurement of its stiffness in the case of flexible base condition; (a) Concrete box; (b) Core-wall

For the fixed condition:

$$\frac{F_{BS}}{V_{Base}} = \frac{210 + 240}{210} = 2.14 \tag{22}$$

And for the flexible bed condition:

$$\frac{F_{BS}}{V_{Base}} = \frac{210 + 699}{210} = 4.33 \tag{23}$$

Now, In order to provide the required parameters in Eq. (12) and Eq. (19) for obtaining of theoretical results, the appropriate related models are considered and are illustrated in Fig. 13 and 14. With these models of the below-grade portion of structures, the calculation of concrete box and core stiffness, as well as the equivalent rotational stiffness at the bottom end core due to flexibility conditions, are truly possible.

The obtained concrete box stiffness values for different cases illustrated in the referenced figures are equal to the following values:

$$\mathrm{K}_{BS} = 862.27\ t/mm \qquad \text{For the case of fixed condition} \tag{24}$$

$$K_{BS} = 474.58\ t/mm \qquad \text{For the case of flexible condition} \tag{25}$$

Comparison of above values obtained from the case of flexible condition with the one with fixed condition shows a considerable difference, which indicates the large impact of the base flexibility on the rate of concrete box stiffness.

The stiffness of the core may be obtained from the case of Fig. 13b. In this model, shear stiffness is highly increased via the features of ETABS program (shell stiffness modification factors). Therefore, the obtained stiffness from the illustrated substructure will account for only the bending stiffness:

$$K_{Core} = 1521.86\ t/mm \tag{26}$$

It is obvious that the core stiffness for the case of flexible condition is also the same value, because the effect of flexibility condition has been considered one time through the term γ.

For the sake of γ calculation, Fig. 14b can be considered. By imposing a lateral load on the core in this model, a moment and a deformation occurs at the bottom end of the core. Measuring the generated mentioned moment and deformations can give the rotational stiffness of the deformable elastic bed:

$$K_{\theta} = 693.4E4\ \frac{T.m}{rad} \tag{27}$$

Now γ can be written as:

$$\gamma = \frac{K_{Core}}{\frac{K_{\theta}}{d^2}} = \frac{1521.9E3}{\frac{693.4E4}{7^2}} = 10.75 \tag{28}$$

The β parameter for a quadrilateral thin walled section can be calculated from the formula of Eq. (14), as well:

$$\beta = 2.4\left(\frac{L_c}{d}\right)^2 = 2.4\left(\frac{6}{7}\right)^2 = 1.763 \tag{29}$$

Now, calculation of the backstay to the lateral force ratio is possible for the two cases of fixed and flexible bed conditions, utilizing the Eqs. of (12) and (18) respectively. From combining Eq. (12) and Eq. (13) for fixed condition:

$$\frac{F_{BS}}{V_{Base}} = \frac{1 + 1.5\frac{\alpha}{1+\beta}\left(\frac{H}{d}\right)}{\frac{K_{Core}}{K_{BS}(1+\beta)} + 1} = \frac{1 + 1.5\frac{0.5}{1+1.763} \times \frac{20 \times 3.5}{7}}{\frac{1521.86}{862.27(1+1.763)}} = 2.27 \tag{30}$$

And by Eq. (18) for a flexible bed condition:

$$\frac{F_{BS}}{V_{Base}} = \frac{1 + \frac{1.5+\gamma}{1+\beta+\gamma}\alpha\left(\frac{H}{d}\right)}{1 + \frac{K_{Core}}{K_{BS}(1+\beta+\gamma)}} = \frac{1 + \frac{1.5+10.75}{1+1.763+10.75} \times 0.5 \times \frac{20 \times 3.5}{7}}{1 + \frac{1521.86}{474.58(1+1.763+10.75)}} = 4.47 \tag{31}$$

Comparison of the results obtained from Eq. (30) and Eq. (31) respectively with the numerical results obtained from Eq. (22) and Eq. (23) shows a good acceptable match.

It is noticeable that, if the cracking (that is a kind of nonlinearity) factor values of contributing

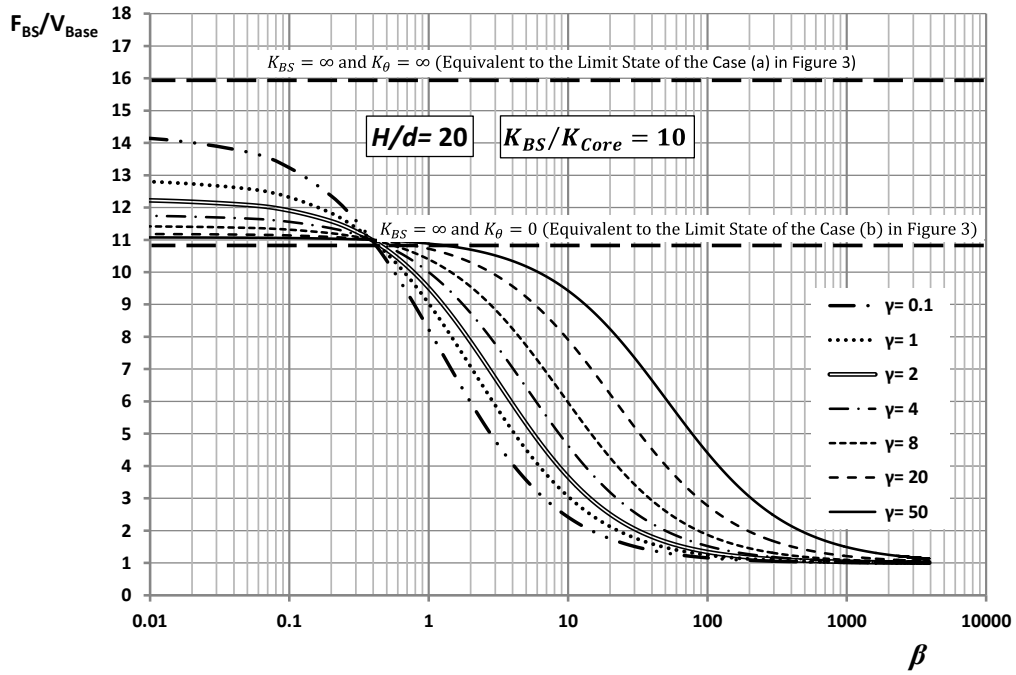

Fig. 15 Variation of backstay force ratio with β parameter, which is showing a special neutral point with respect to γ

components in Eq. (18) or (19) be designated, the mentioned equations can be used directly for determining the outcome of these cracking effects.

3.2 More Inspecting of the new proposed relationship

A presentation of the variation of F_{BS}/V_{Base} with the relative rotational stiffness of γ was shown at previous section. However, an investigation of this variation with β (or d/L_C) can also be interesting. For this sake, the variation of F_{BS}/V_{Base} with β, for constant parameters of H/d=20, K_{BS}/K_{Core}=10, and a uniformly distributed lateral load (α=0.5) is presented in Fig. 15. Some interesting points are noticeable in this figure. The first remarkable note is when the ratio of d/L_C is increased enough (or the β is decreased), the curve ends approach to one of the limit states described previously. It is evident that for the small values of γ, the values of F_{BS}/V_{Base} approach to the upper limit state presented in Fig. 3 (case (a) in this figure). A similar trend can be observed, where for the large values of γ, the values of the vertical axis approach to the lower limit state of Fig. 3 (case (b) in this figure). These observations confirm the compatibility of the results of the new relationship with the results of the previous primary research.

Another and a more interesting observable matter in this figure is the existence of a point at which all curves intersect each other. This fact signifies the existence of a special point at which the γ values have no effect upon the results and can be interpreted as a point with no sensitivity to the K_θ.

If the referred point is named as “neutral point", solution for obtaining it gives the following expression:

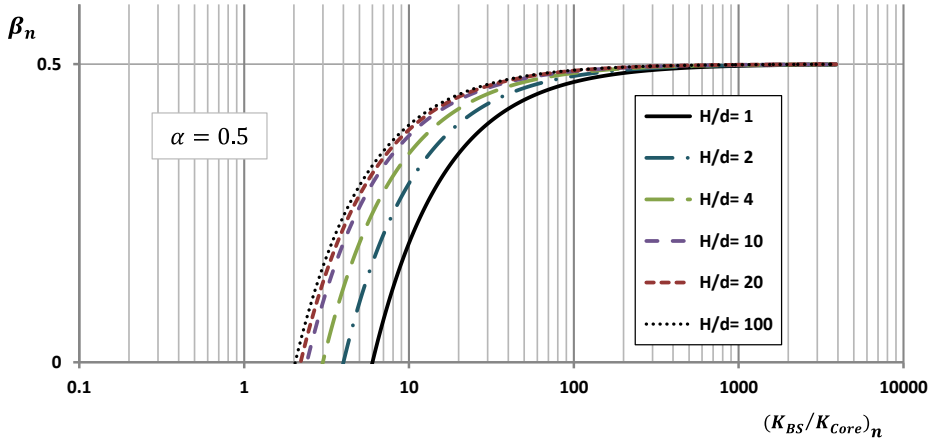

Fig. 16 Rapidly matching of the neutral point for a rather high value of H/d

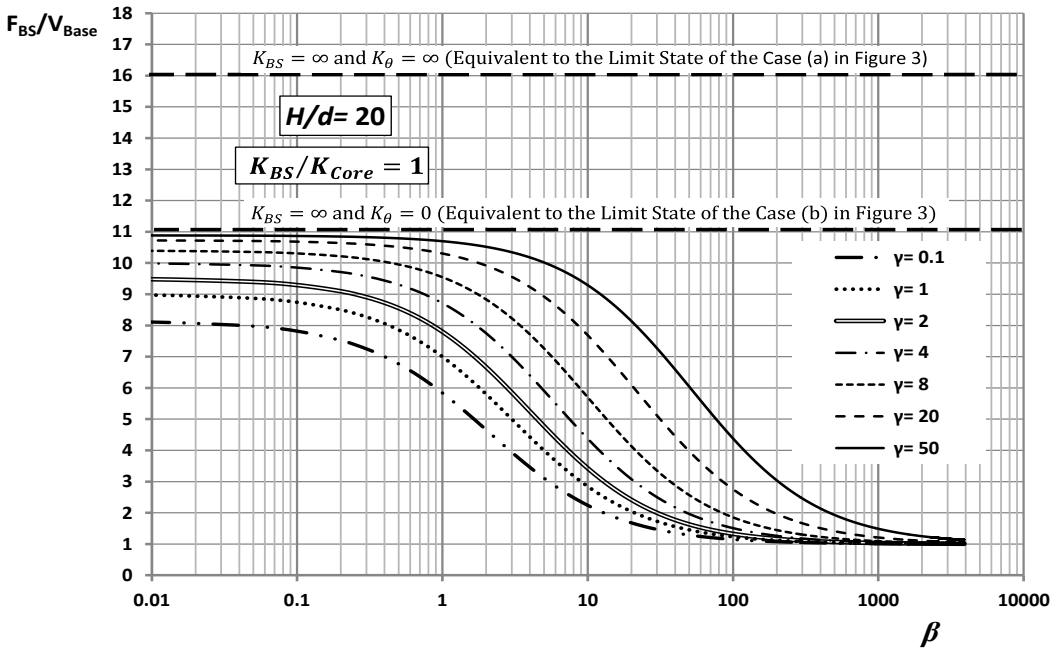

Fig. 17 Illustration of a case for K_{Core}/K_{BS} that is bigger than 0.5 value is showing that the curves do not intersect with each other and all the values of F_{BS}/V_{Base} are less than the limit state of the case (b) in Fig. 3

$$\beta_n = \frac{\left[0.5 - \left(\frac{K_{Core}}{K_{BS}}\right)_n\right]\alpha\left(\frac{H}{d}\right) - \left(\frac{K_{Core}}{K_{BS}}\right)_n}{\alpha\left(\frac{H}{d}\right)} \tag{32}$$

Investigation of this relation, as shown in Fig. 16, implies that with increasing the ratio of H/d , the curves are matching to each other rapidly. Therefore, for the high ratio of H/d (about H/d≥10),

that is true for almost all tall buildings, the latter equation may be reduced to the one below:

$$\beta_n = 0.5 - \left(\frac{K_{Core}}{K_{BS}}\right)_n \tag{33}$$

This equation also yields the result that the mentioned special point is conceivable only when the K_{Core}/K_{BS} is less than 0.5 value. In other words, when the ratio of K_{Core}/K_{BS} is bigger than 0.5, then the curves do not ever intersect with each other. An example of these cases is illustrated at Fig. 17 for the value of 1 for the ratio of K_{Core}/K_{BS}. It can also be noted that when this ratio in Fig. 17 is bigger than 0.5, the F_{BS}/V_{Base} ratio will be less than the value of limit state case of Fig. 3b $(1+\alpha(H/d))$.

3.3 Regularization of the proposed equation

Due to existence of many parameters in the proposed equation, Eq. (18), and consequently, a probable confusing situation, as well as the aim for regularization of this equation for using in applicable circumstances, the particular conditions affecting the ratio of F_{BS}/V_{Base} have been classified and presented here.

At first, it can be said that under any condition (certainly based on supposed discussed assumptions particularly ignoring the inertia forces in the subterranean levels for seismic loads) the F_{BS}/V_{Base} ratio never exceeds $1+1.5\alpha(H/d)$. This condition is occurred when the stiffness of foundation, K_θ, and concrete box, K_{BS}, are very larger than the core-wall stiffness, provided that the β parameter is rather small. Consequently, this may be imagined as the extreme worst condition for the core-wall that may occur.

Another noteworthy case is the condition that the F_{BS}/V_{Base} ratio is less than one. This condition occurs when the following expression is governed:

$$\frac{K_{Core}/K_{BS}}{1.5+\gamma} > \alpha\frac{H}{d} \tag{34}$$

Expression above shows that the β parameter has no impact on this specific considered condition.

Another significant case may be related to the neutral point. As indicated, at this point the value of F_{BS}/V_{Base} will be equal to $1+\alpha(H/d)$. Furthermore, for a high-rise building, it was seen that the expression for the neutral point was reduced to a simpler form. By utilization the mentioned expression for tall buildings, one can now determine a condition that the ratio of F_{BS}/V_{Base} is within a specific range. This attempt leads to the following specific condition:

$$\frac{K_{Core}}{K_{BS}} + \beta < 0.5 \qquad \Rightarrow \qquad 1+\alpha\frac{H}{d} < \frac{F_{BS}}{V_{Base}} < 1+1.5\alpha\frac{H}{d} \tag{35}$$

The last considered case is excluding any of the previous cases, which automatically produces the following condition:

$$\begin{cases} \dfrac{K_{Core}/K_{BS}}{1.5+\gamma} < \alpha\dfrac{H}{d} \\ \quad and \\ \dfrac{K_{Core}}{K_{BS}} + \beta > 0.5 \end{cases} \qquad \Rightarrow \qquad 1 < \frac{F_{BS}}{V_{Base}} < 1+\alpha\frac{H}{d} \tag{36}$$

These presented regularized cases for various conditions can help structural designers make a proper decision for the aspect ratio value of the below-grade structural elements with respect to backstay effect. The presented relationships may have significant roles from a standpoint of control skills (mostly passive control) as well.

4. Conclusion

In this research, attempted to obtain a relationship for prediction of backstay force based on relative stiffness of the structural components, composing the underground portion of building. The main obtained results from this research are as follows:

- The proposed Eq. (18) is a development of the previous equations for prediction of backstay effects. This expression, not only maintains the compatibility with the earlier relationships, but is also capable of considering more involving parameters (foundation flexibility effect) for the sake of evaluation of backstay effects.
- The presentation of the proposed equation in a non-dimensional form, including the ratio of α, β, γ, and K_{Core}/K_{BS} can create a more conceptual insight for realizing the involved parameters in the backstay effect.
- Although the given formula has been obtained for a linear elastic condition, a series of proper reduction factors due to cracking may be applied directly to the stiffness ratios such as K_{Core}/K_{BS} and etc. for consideration of cracking and some nonlinearity effects.
- The presented regularized equation may help structural engineers select an appropriate aspect ratio for the below-grade structural elements. This can be achieved by knowledge or investigation of the specific of the Moment/Shear ratio for the best behavior of shear walls.
- A special point named “neutral point” as discussed can be used as a particular point at which the sensitivity of the structural response might be reduced with respect to some of the parameters that may cause the variations in the mechanical characteristics of the below-grade structural elements due to any sources of nonlinearity.
- If the main backstay diaphragm is modeled as a rigid diaphragm, it causes an artificial increase in the concrete box stiffness, K_{BS}. Referring to the proposed equation, a larger backstay force affecting the core-wall is resulted, with no effect on the backstay diaphragm. Therefore and in the modeling process, application of a semi-rigid diaphragm must be considered for achieving realistic results.

References

Adebar, P. (2008), “Design of high-rise core-wall buildings: A Canadian perspective”, *Proceedings of the 14th World Conference on Earthquake Engineering*, Beijing, China, October.

Beiraghi, H., Kheyroddin, A. and Kafi, M.A. (2016), “Forward directivity near-fault and far-fault ground motion effects on the behavior of reinforced concrete wall tall buildings with one and more plastic hinges”, *Struct. Design Tall Special Buildings*, **25**(11), 519-539. https://doi.org/10.1002/tal.1270.

Beiraghi, H. (2018a), “Energy demands in reinforced concrete wall piers coupled by buckling restrained braces subjected to near-fault earthquake”, *Steel Compos. Struct.,* **27**(6), 703-716. https://doi.org/10.12989/scs.2018.27.6.703.

Beiraghi, H. (2018b), “Energy dissipation of reinforced concrete wall combined with buckling-restrained braces subjected to near- and far-fault earthquakes”, *Iran. J. Sci. Technol., Transactions Civil Eng.*, **42**(4),

345–359. https://doi.org/10.1007/s40996-018-0109-0.
Beiraghi, H. (2018c), "Near-fault ground motion effects on the responses of tall reinforced concrete walls with buckling-restrained brace outriggers", *Scientia Iranica*, **25**(4), 1987-1999. https://dx.doi.org/10.24200/sci.2017.4205.
Beiraghi, H. (2018d), "Reinforced concrete core-walls connected by a bridge with buckling restrained braces subjected to seismic loads", *Earthq. Struct.,* **15**(2), 203-214. https://doi.org/10.12989/eas.2018.15.2.203.
Beiraghi, H. (2017), "Earthquake effects on the energy demand of tall reinforced concrete walls with buckling-restrained brace outriggers", *Struct. Eng. Mech.,* **63**(4), 521-536. https://doi.org/10.12989/sem.2017.63.4.521.
Beiraghi, H. and Siahpolo, N. (2016), "Seismic assessment of RC core-wall building capable of three plastic hinges with outrigger", *Struct. Design Tall Special Buildings,* **26**(2), 1306-1325. https://doi.org/10.1002/tal.1306.
Farghaly, A. A. (2016), "Seismic assessment of slender high rise buildings with different shear walls configurations", *Adv. Comput. Design,* **1**(3), 221-234. https://doi.org/10.12989/acd.2016.1.3.221.
Fu, F. (2018), *Design and Analysis of Tall and Complex Structures,* Elsevier Science, Cambridge, MA, USA.
Fu, F. (2015), *Advanced Modeling Techniques in Structural Design*, Wiley, West Sussex, Chichester, UK.
Gere, J.M. and Timoshenko, S.P. (1991), *Mechanics of Materials,* 3rd Edition, Springer, New York, USA.
Karimi, M. and Kheyroddin, A. (2016), "Study of backstay effect in tall buildings and presentation of governed relationships of structural behavior from this standpoint", *2nd National Conference of Iranian structural Engineering*, Tehran, Iran, February.
Karimi, M., Kheyroddin, A. and Shariatmadar, H. (2018), "Study of Backstay Effect in Tall Buildings with Core Wall System by Involving of Shear Deformation", *Bullet. Earthq. Sci. Eng.*, **5**(3), 61-71.
Kowalczyk, R.M., Sinn, R., Bennetts, I.D. and Kilmister, M.B. (1995), *Structural Systems for Tall Buildings*, Council on Tall Buildings and Urban Habitat, McGraw-Hill, New York, USA.
LATBSDC (2017), *An Alternative Procedure for Seismic Analysis and Design of Tall Buildings Located in the Los Angeles Region 2017 Edition*, Los Angeles Tall Buildings Structural Design Council; Los Angeles, CA, USA.
Moehle, J. (2015), *Seismic Design of Reinforced Concrete Buildings*, McGraw-Hill Education, New York, USA.
PEER/ATC-72-1 (2010), "Modeling and Acceptance Criteria for Seismic Design and Analysis of Tall Buildings", PEER Rep. No. 2010/111, Pacific Earthquake Engineering Research Center, Berkeley, CA, USA.
Rad, R.B. and Adebar, P. (2009), "Seismic design of high-rise concrete walls: Reverse shear due to diaphragms below flexural hinge", *J. Struct. Eng.*, **135**(8), 916-924. https://doi.org/10.1061/(ASCE)0733-9445(2009)135:8(916).
Smith, B.S. and Coull, A. (1991), *Tall Building Structures: Analysis and Design,* John Wiley & Sons, New York, USA.
Taranath, B.S. (2010), *Reinforced Concrete Design of Tall Buildings,* CRC Press, Taylor & Francis, Boca Raton, Florida, USA.
TBI/PEER (2017), "Tall Building Initiative, Guidelines for Performance-Based Seismic Design of Tall Buildings", PEER 2017/06, Pacific Earthquake Engineering Research Center; Berkeley, CA, USA.
Tocci, N. and Levi, S. (2012), "Basement modeling in tall buildings: Backstay effect", *Structure Magazine*, **June**, 23-24.

CC